




Open Archive Toulouse Archive Ouverte (OATAO)

OATAO is an open access repository that collects the work of Toulouse researchers and makes it freely available over the web where possible

This is a Publisher's version published in: <http://oatao.univ-toulouse.fr/26973>

Official URL: <https://doi.org/10.1002/ejic.202000436>

To cite this version:

Beer, Sebastian M. J. and Krusenbaum, Annika and Winter, Manuela and Vahlas, Constantin  and Devi, Anjana *Study on Structural and Thermal Characteristics of Heteroleptic Yttrium Complexes as Potential Precursors for Vapor Phase Deposition*. (2020) *European Journal of Inorganic Chemistry*, 2020 (37). 3587-3596. ISSN 1434-1948

Any correspondence concerning this service should be sent to the repository administrator: tech-oatao@listes-diff.inp-toulouse.fr

ALD Precursors

Study on Structural and Thermal Characteristics of Heteroleptic Yttrium Complexes as Potential Precursors for Vapor Phase Deposition

Sebastian M. J. Beer,^[a] Annika Krusenbaum,^[a] Manuela Winter,^[a] Constantin Vahlas,^[b] and Anjana Devi*^[a]

Abstract: Yttrium oxide (Y₂O₃) thin films are implemented as a functional component in a broad field of applications such as optics, electronics or thermal barrier coatings. Atomic layer deposition (ALD) is a promising technique to fabricate high-quality thin films with atomic level precision in which the precursor choice plays a crucial role in process development. The limited number of suitable yttrium precursors available for ALD of Y₂O₃ has triggered increasing research activity seeking new or modified precursors. In this study, heteroleptic compounds of yttrium bearing the cyclopentadienyl (Cp) ligand in combination with the chelating amidinate or guanidinate ligands were targeted as potential precursors for ALD. In this context, a systematic and comparative study of the structure and thermal characteristics of (bis-cyclopentadienyl-(*N,N'*-diisopropyl-2-

methyl-amidinato)yttrium) [YCp₂(dpamd)] **1** and (bis-cyclopentadienyl-(*N,N'*-diisopropyl-2-dimethylamido-guanidinato)yttrium) [YCp₂(dpdmg)] **2** was performed. Complementary characterization tools such as ¹H-NMR, elemental analysis, electron-impact mass spectrometry (EI-MS) and single-crystal X-ray diffraction (XRD) confirmed the spectroscopic purity and the monomeric nature of the metalorganic compounds. Hirshfeld surface analysis revealed influence of the ligand choice on the intermolecular interactions of the compounds. The important figures of merit for a precursor, namely the thermal properties were investigated via thermogravimetric analysis. Thus, the volatility, transport behavior and thermal stability were examined and compared to their homoleptic counterparts [YCp₃], [Y(dpamd)₃] or [Y(dpdmg)₃].

Introduction

Over the years, rare-earth oxides (REO) have been regarded as a promising class of materials which can be implemented in the form of powders^[1] nanoparticles^[2] or thin films^[3] for a multitude of applications. Especially, due to their large band gap (5.5 eV) and high refractive index (ca. 2.0), yttrium oxide (Y₂O₃) and rare-earth (RE) doped Y₂O₃ like Ce³⁺:Y₂O₃ or Nd³⁺:Y₂O₃ exhibit outstanding potential in the field of optics such as lasers,^[4] planar waveguides^[5] or antireflective coatings.^[6] Moreover, the high relative permittivity of Y₂O₃ (ε_r ca. 17–20)^[7] makes it suitable as high-κ dielectric material in complementary metal oxide semiconductor (CMOS)-based de-

vices. Owing to the superior thermal robustness and low heat transition rate, yttria-stabilized zirconia (YSZ)^[8] and layered Y₂O₃ ceramics^[9] function as high-performance thermal barrier coatings (TBC) on turbine blades.^[10] Besides, they perform well as corrosion protection layers due to their chemical durability in harsh environments.^[11]

A variety of vapor phase deposition techniques have been utilized in the past to deposit thin films of Y₂O₃, RE:Y₂O₃ and YSZ, covering physical methods such as molecular beam epitaxy (MBE),^[12] sputtering^[6c,13] or pulsed laser deposition (PLD).^[14] Alternatively, chemical vapor deposition (CVD)^[15] and especially atomic layer deposition (ALD)^[3b,3c,16] have gained more attention recently. This is especially applicable to latter technique as it enables coating on large areas and three-dimensional geometries with excellent uniformity, precise thickness control and conformity based on the self-limiting nature of the process. These attributes have resulted in the application of ALD processing in various technological sectors.^[17]

The ALD process is strongly influenced by the physicochemical characteristics of the employed precursor. One particular feature is the reactivity of the precursor which necessitates the employment of suitable ligands that meet the requirements of an ALD process.^[18] Apart from the reactivity and volatility, an "ideal" ALD precursor should also feature a good thermal stability that is of high relevance to avoid any CVD-type contribution to the overall film growth. In this context, chelating ligands

[a] S. M. J. Beer, A. Krusenbaum, M. Winter, Prof. A. Devi
Inorganic Materials Chemistry, Faculty of Chemistry and Biochemistry,
Ruhr University Bochum,
Universitätsstr. 150, 44801 Bochum, Germany
E-mail: anjana.devi@rub.de
<https://imc.ruhr-uni-bochum.de/>

[b] Dr. C. Vahlas
Centre Inter-Universitaire de Recherche et d'Ingénierie des Matériaux -
CNRS, Université de Toulouse,
Allée Emile Monso, BP-44362, 31030 Toulouse Cedex 4, France

Supporting information and ORCID(s) from the author(s) for this article are available on the WWW under <https://doi.org/10.1002/ejic.202000436>.

© 2020 The Authors published by Wiley-VCH GmbH · This is an open access article under the terms of the Creative Commons Attribution License, which permits use, distribution and reproduction in any medium, provided the original work is properly cited.

show more promise as the coordination of the large ionic radius of the RE metal center can be saturated. Moreover, the volatility and reactivity of the precursors can be altered by the choice and combination of employed ligands. The variation of their steric bulk allows further fine-tuning of the physicochemical properties. Both strategies directly influence the intermolecular and intramolecular interactions present in the resulting precursor. To make a potential precursor appealing for ALD, facile synthesis scale-up as well as straightforward purification procedures are desired. Although it is challenging to satisfy all the above-mentioned requirements, targeted exploratory studies on metalorganic compounds can pave the way to find an improved precursor for ALD applications fulfilling most of them.

Generally, the unique chemistry associated with the RE elements, and particularly yttrium should be considered in the process of developing new precursors. A range of different synthesis strategies for the formation of new organoyttrium complexes has been established over the last years to synthesize promising complexes that could be useful in catalysis or for materials synthesis.^[19] Depending on the synthon e.g. metallic Y, YCl₃ or organolanthanides, the desired complexes are accessible via salt metathesis, salt elimination, transmetallation, metal vapor synthesis or ligand exchange routes.^[20] However, based on the unique chemical and electronic nature, the formation of yttrium complexes is not directly comparable to the transition metal chemistry of the *d*-block elements. Characteristics such as the large ionic radius, the favored oxidation state of +3 and the stabilization of highly coordinated complexes need to be considered when designing and developing yttrium-containing ALD precursors. Moreover, yttrium possesses a low electronegativity resulting in the formation of metal-ligand bonds with a predominantly ionic character. As a hard acid following the *hard and soft acids and bases* concept (HSAB), yttrium and RE elements in general prefer hard ligands such as halides or ligand systems possessing N or O coordination which further explains the hygroscopic nature of the RE containing compounds. However, it was found out that the bond lability is based on kinetically favored reactions since from a thermodynamically perspective, the RE-ligand bonds provide sufficient stability.^[21]

Focusing on the established Y-precursors for ALD, [Y(thd)₃] (thd: 2,2,6,6-tetramethyl-3,5-heptanedione) is a prominent example which is thermally stable and possesses moderate volatility. Yet, its reactivity toward water is limited necessitating the use of ozone or oxygen as co-reagent and high temperatures for depositions.^[22]

Another well-established ligand class for yttrium complexation is the cyclopentadienyl ligand (Cp) [C₅H₅]⁻ which provides a delocalized π -system typically resulting in an η^5 -bonding to the metal center. Due to the conjugated five-membered aromatic ring this system features a high thermal stability. In particular, the Cp substituted rare-earths are prone to hydrolysis due to their strong Brønsted base character rendering them suitable for ALD using H₂O as mild oxidizing agent as demonstrated for the growth of Y₂O₃.^[23] A variation of the Cp ligands yields complexes of the type [Y(RCp)₃], (R = Me, Et, *i*Pr, *t*Bu) with decreasing melting points based on the higher degree of asymmetry and thus hindered rotation of the Cp moieties re-

sulting in a limitation of intermolecular interactions. However, in some cases the reported ALD processes were not entirely self-limiting and required high deposition temperatures.^[16a,23b,24]

Other classes of precursors that have gained significant attention within the ALD community are the all-N coordinated amidinates and guanidinates of yttrium which are considered superior ALD precursors for Y₂O₃ thin films. These ligand classes feature an η^2 bidentate bonding mode satisfying the coordination chemistry of the RE which possess large ionic radii. The NCN backbone unit provides a π -delocalized character which enhances the stability of the ligand skeleton. In addition, the presence of the reactive RE–N bonds imparts higher reactivity compared to the thd ligand, thus enabling ALD at low temperatures using water as co-reactant.^[3c,19b,25] Furthermore, the versatility of the homoleptic amidinate and guanidinate class was also demonstrated for its implementation in metalorganic chemical vapor deposition (MOCVD) of REO, REN and RES thin films.^[26]

Lately, the rational development of heteroleptic precursors has been in focus of ALD research. The introduction of different ligand moieties is expected to strongly affect the symmetry of a complex. This, in turn can influence the intermolecular interactions resulting in decreased melting points and in an optimal case, increased volatility compared to homoleptic analogues thus paving the way for improved precursors. One representative example is the combination of cyclopentadienyl and amidinate ligands resulting in heteroleptic rare-earth complexes of the type [RE(RCp)₂(dpamd)] (dpamd = *N,N'*-diisopropyl-2-methyl-amidinato) with R = H, Me, Et, *i*Pr.^[27] This class of compounds was found to possess beneficial physicochemical properties such as lowering of melting points down to room temperature and high reactivity toward water. The utility of these compounds in ALD processes for RE₂O₃ (RE = Y, La, Pr, Gd and Dy) and Y:HfO₂ thin films were recently demonstrated.^[3b,16b–16g]

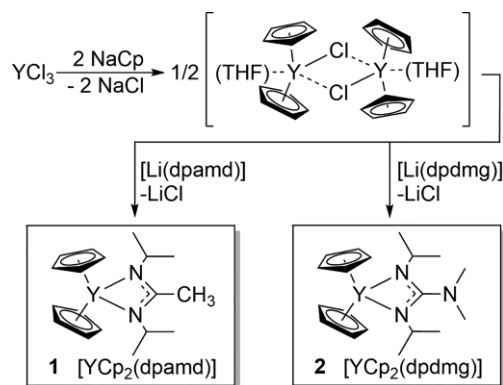
Although [RE(RCp)₂(dpamd)] complexes have been successfully used for ALD of the respective RE₂O₃, till date there has been no study carried out focusing on the thorough evaluation of the compounds and understanding the influence of structural parameters on physicochemical properties. Such systematic research on precursor chemistries is needed as it enables to gain fundamental insights that are crucial to design new and promising precursors rather than implement trial and error strategies for ALD process development.

This prompted us to extend the precursor library available for yttrium through the inclusion of the mixed guanidinate [YCp₂(dpdmg)] **2** compound (dpdmg = *N,N'*-diisopropyl-2-dimethylamido-guanidinato). Furthermore, we compare the precursor characteristics to the reported amidinate analogue, namely [YCp₂(dpamd)] **1**. It should be noted here that [YCp₂(dpamd)] **1** has been reported in a patent^[27] but no detailed precursor analysis has been disclosed so far. In order to investigate the role of the ligand substitution on the intermolecular interactions we used Hirshfeld surface analysis which allowed a correlation to the thermal characteristics between the different complexes. For a thorough understanding of the thermal properties of the two complexes a benchmark with

the homoleptic counterparts namely $[\text{YCp}_3]$, $[\text{Y}(\text{dpamd})_3]$ and $[\text{Y}(\text{dpdmg})_3]$ was performed. Thus, this study encompasses a comparison of the thermal properties amongst the heteroleptic mixed Cp-amidates, mixed-Cp guanidates and the homoleptic Cp classes of Y precursors.

Results and Discussion

Metalorganic yttrium complexes are accessible using different synthetic approaches. In this study, a salt-metathesis reaction with YCl_3 as a starting material was adopted. The halide salt was treated with organosodium and organolithium reagents to form the target complexes. While the homoleptic counterparts $[\text{YCp}_3]$, $[\text{Y}(\text{dpamd})_3]$ and $[\text{Y}(\text{dpdmg})_3]$ were synthesized following literature procedures,^[3e,25,28] the syntheses of the heteroleptic compounds $[\text{YCp}_2(\text{dpamd})]$ **1** and $[\text{YCp}_2(\text{dpdmg})]$ **2** were performed modifying a procedure reported earlier for **1** (Scheme 1).^[27] The resulting compounds **1** and **2** were obtained after sublimation with moderate yields of 45 % and 52 %, respectively. Purification was carried out through sublimation yielding X-ray quality crystalline solids. The intermediate compound $[(\text{THF})\text{Cp}_2\text{YCl}_2]$ was isolated and characterized by $^1\text{H-NMR}$ and single-crystal analysis as well. The structure is shown in Figure S1 in the Supporting Information.



Scheme 1. General synthesis scheme for the formation of $[\text{YCp}_2(\text{dpamd})]$ **1** and $[\text{YCp}_2(\text{dpdmg})]$ **2**.

Single Crystal X-ray Diffraction and NMR Spectroscopy

The structural geometries of metalorganic complexes can strongly influence their physicochemical behavior. Through a better understanding of structural features e.g. bonding, nuclearity, hapticity of the chelate or ligand distortion and the evaluation of the resulting physicochemical characteristics of the precursor, valuable correlations can be made that can guide rational precursor design and thus tuning the properties relevant for ALD. One powerful tool is the single-crystal analysis as it provides insight into the structure of the molecule.

Crystals suitable for single-crystal X-ray diffraction were obtained by sublimation of **1** and **2**. The crystal structures and crystallographic data refinement are depicted in Figure 1 and Table 1, respectively. From the single crystal XRD measurements, both $[\text{YCp}_2(\text{dpamd})]$ **1** (CCDC 1986425) and

$[\text{YCp}_2(\text{dpdmg})]$ **2** (CCDC 1986424) feature similar structural characteristics such as a monomeric nature in the solid state, crystallizing in the orthorhombic crystal system with a $P2_12_12_1$ space group and a coordination geometry which can be best described as pseudo-tetrahedral.

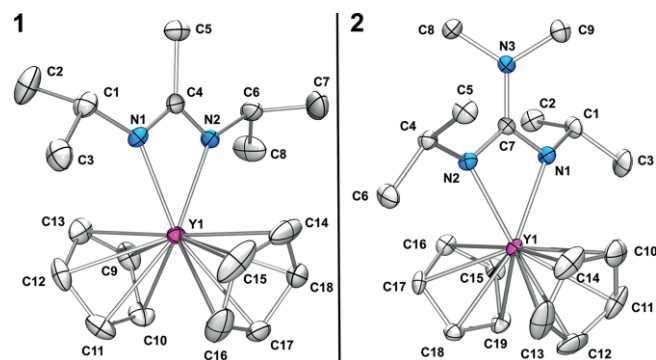


Figure 1. Solid-state structure of compound $[\text{YCp}_2(\text{dpamd})]$ **1** (left, CCDC 1986425) and $[\text{YCp}_2(\text{dpdmg})]$ **2** (right, CCDC 1986424). H Atoms are omitted for the sake of clarity, thermal ellipsoids represent 30 % probability.

Table 1. Crystallographic data for compound $[\text{YCp}_2(\text{dpamd})]$ **1** and $[\text{YCp}_2(\text{dpdmg})]$ **2**.

	$[\text{YCp}_2(\text{dpamd})]$ 1	$[\text{YCp}_2(\text{dpdmg})]$ 2
Empirical formula	$\text{C}_{18}\text{H}_{27}\text{N}_2\text{Y}$	$\text{C}_{19}\text{H}_{30}\text{N}_3\text{Y}$
M (g/mol)	360.32	389.37
T [K]	100.00(10)	147(60)
Radiation	Cu K_{α} ($\lambda = 1.54184$)	Mo K_{α} ($\lambda = 0.71073$)
Crystal size/mm ³	0.24 × 0.1 × 0.08	0.24 × 0.19 × 0.100
Crystal system	orthorhombic	orthorhombic
Space group	$P2_12_12_1$	$P2_12_12_1$
a [Å]	21.6614(5)	9.3936(4)
b [Å]	9.6011(2)	12.6073(6)
c [Å]	8.6343(2)	16.3737(10)
α (°)	90	90
β (°)	90	90
γ (°)	90	90
V [Å ³]	1795.70(7)	1939.12(17)
Z	4	4
ρ_{calc} (g/cm ³)	1.333	1.334
μ [mm ⁻¹]	4.518	3.011
Data/restraints/parameters	3479/0/195	4711/0/214
2 θ range (°)	8.164 to 148.58	4.976 to 61.618
Unique reflections	3479	4711
	[$R_{\text{int}} = 0.0225$]	[$R_{\text{int}} = 0.0464$]
	[$R_{\text{sigma}} = 0.0213$]	[$R_{\text{sigma}} = 0.0550$]
GOF on F^2	1.061	1.033
Final R indexes [$I \geq 2\sigma(I)$]	$R_1 = 0.0198$	$R_1 = 0.0388$
	$wR_2 = 0.0499$	$wR_2 = 0.0965$
Final R indexes [all data]	$R_1 = 0.0224$	$R_1 = 0.0466$
	$wR_2 = 0.0503$	$wR_2 = 0.1021$
Largest diff. peak/hole (e Å ⁻³)	0.20/−0.39	0.99/−0.76

This bent-sandwich like configuration^[29] forms Y–N σ -bonds from the η^2 -chelating guanidinate or amidinate ligand and π -bonds between the Cp units and Y.^[19b]

The average Y–N bond lengths were found to be 2.312 Å and 2.316 Å for **1** and **2** similar to those reported for structurally related compounds such as $[\text{Y}(\text{dpdmg})_3]$ (2.368 Å).^[3e]

The NCN backbone of the amidinate (N1–C4–N2) and guanidinate (N1–C7–N2) ligands exhibits C–N bond lengths in

the range between single and double bonds indicating a delocalized character of the system. Interestingly, this phenomenon is also observed for the C-NMe₂ function of the guanidinate ligand of **2** which features a shortened C-NMe₂ bond. Ideally, the methyl groups of the sp²-hybridized N3 center are oriented in the same plane as the N atoms of sp²-hybridized backbone C7 to ensure a perfect π -orbital overlap. However, a twist of the C-NMe₂ moiety of 36.43° hinders the N to push enough electron density to the C π -orbital. The influence of the higher steric demands of the twisted NMe₂ group of **2** compared to the less hindered CH₃ group of **1** can further be elucidated focusing on the Dieder-angle of the isopropyl groups bonded to the N of the NCN functions spanning angles of 23.42° for C1-N1-N2-C4 (compound **1**) and 75.36° for C1-N1-N2-C6 (compound **2**), respectively.

The bond length between the Cp units and the metal center are comparable to the results of analogous Cp containing Y complexes as for instance [Y(Cp₃)].^[30] The Q₁-Y1-Q₂ angle (Q₁ and Q₂ = centroids in a Cp ring) for **1** was found to be 130.05° whereas the value for **2** was calculated to be smaller being 126.84°. This slight difference is most probably due to the lower steric interaction of the CH₃ group of the NCN backbone of **1** which allows more space to the N-bonded isopropyl functions and consequently to the Cp groups.

¹H-NMR was conducted to gain insight into the purity of the synthesized compounds and their structural characteristics. Based on the findings depicted in Figure 2, it is evident that both compounds **1** and **2** retain the monomeric nature when dissolved in benzene. All integrals and signals can be unambiguously assigned to the expected structures of the complexes. The protons of the Cp units (signal **a**) in both complexes are chemically equivalent and due to the aromaticity of the ring-system, the proton signal is shifted downfield to 6.20 ppm for complex **1**, and 6.24 ppm for **2**. The central proton **c** of the *i*Pr function couples as a doublet of septet, shifted to 3.24 ppm and 3.39 ppm for **1** and **2**, respectively. The coupling constants of $J = 6.3$ Hz for the septets can be assigned to the coupling with the neighboring protons of the methyl moieties of the *i*Pr function, whereas the comparably smaller constant of $J = 2$ Hz is reasoned by a ³*J* coupling of these protons with the Y metal center.

The methyl groups of the *i*Pr substitutions (signal **b**) form a clear doublet with $J = 6.3$ Hz which is shifted high field to approximately 1 ppm. From previous studies on the homoleptic [Y(dpdmg)₃] analogue, it was shown that two distinguishable doublets were obtained for these methyl moieties of the *i*Pr groups. This can be explained by a slow rotation of the *i*Pr groups compared to the NMR timescale reasoned by steric hindrance of adjacent ligand groups and the dimethylamido function. For the heteroleptic counterpart [YCp₂(dpdmg)] **2** this phenomenon is not observed which is a consequence of the lower steric hindrance enforced by the Cp units resulting in a free rotation of the *i*Pr groups. The backbone methyl group protons of **1** and dimethylamido group signals of **2** (both signal **d**) can be found at $\delta = 1.44$ ppm and $\delta = 2.35$ ppm, respectively. The shift to low field regime for the signal of **2** can be explained by the stronger delocalized character of the NCN function which withdraws the electrons of the methyl functions of this unit.

In summary, the successful formation of the target compounds **1** and **2** was confirmed via single crystal analysis and ¹H-NMR spectroscopy, wherein the monomeric nature is retained both in the solid state and solution.

Mass Spectrometry

Electron-impact mass spectrometry (EI-MS) measurements were conducted to further confirm the formation of the compounds and to elucidate the stabilities of the yttrium complexes under harsh ionization conditions (Figure 3).

The detection of the molecular ion peaks [M]⁺ at 360.1 *m/z* (52.3 %) and 389.2 *m/z* (59.8 %) for **1** and **2** corroborates the formation of the expected yttrium complexes. Additionally, from the high relative intensity of the molecular ion fragments of >50 %, it can be concluded that the compounds possess a high stability with respect to extreme ionization conditions.

From the obtained MS spectra, possible fragmentation patterns were postulated for **1** and **2** as depicted in Figure 3 (left). Both compounds feature a similar molecular structure only differing in the substitution located at the NCN backbone leading to a similar fragmentation behavior. Firstly, the absence of nu-

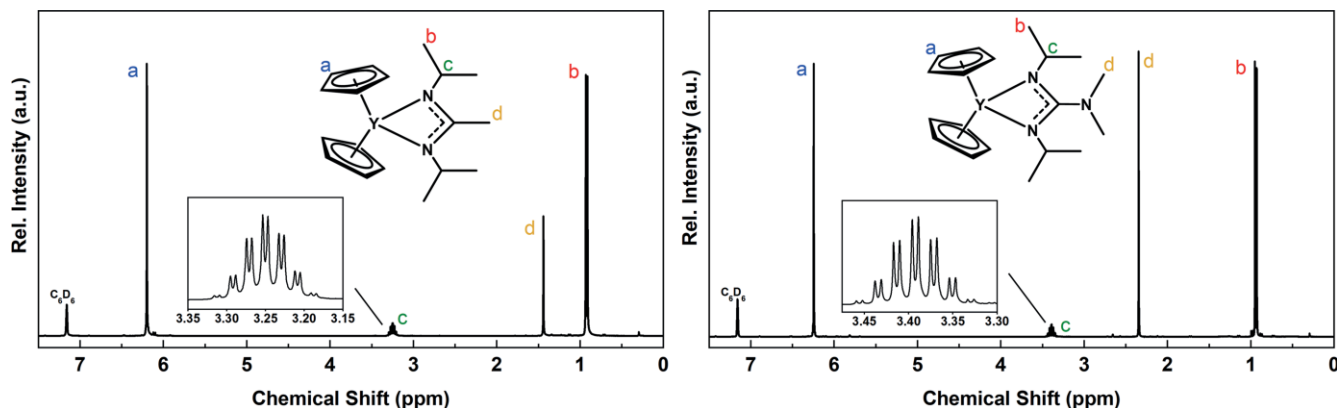


Figure 2. ¹H-NMR of compound [YCp₂(dpamd)] **1** (left) and [YCp₂(dpdmg)] **2** (right). Insets show the magnification of the doublets of septets.

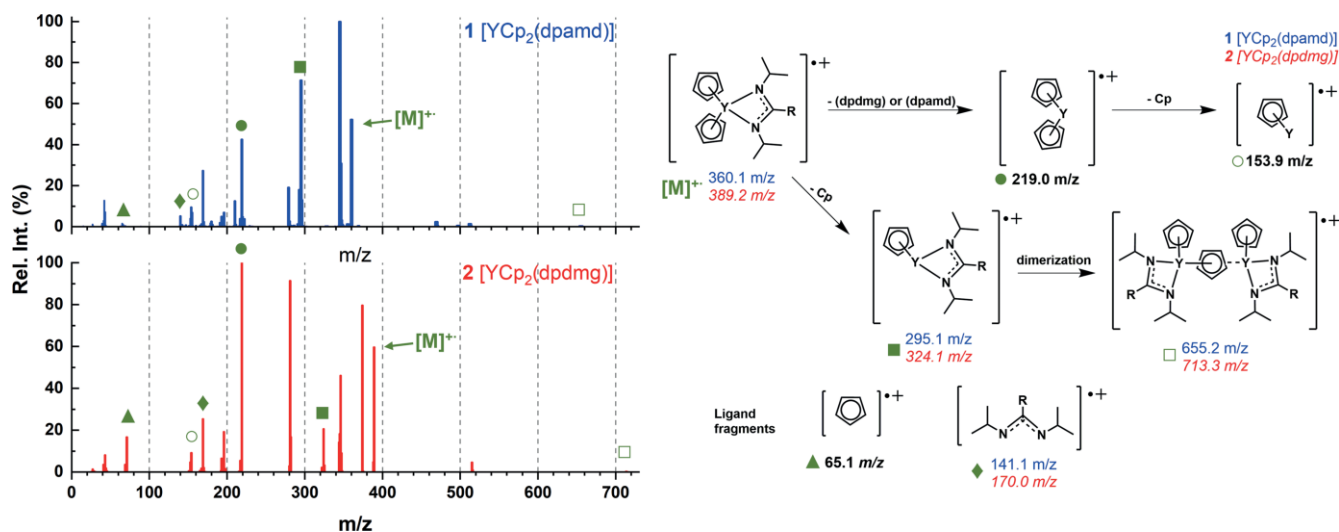


Figure 3. EI-MS spectra (left) of [YCp₂(dpamd)] **1** (R = Me in blue) and [YCp₂(dpdmg)] **2** (R = NMe₂ in red) in combination with the respective proposed fragmentation pattern for **1** and **2** (right). The *m/z* values of the respective fragments are listed in blue for **1**, red (italic) for **2** and black (bold) for similar values.

merous fragments with low relative intensities suggests the cleavage of intact ligand moieties such as Cp, dpamd or dpdmg underlining the remarkable stability of these substituents even upon ionization. From [M]⁺⁺, the loss of an intact amidinate or guanidinate ligand facilitates the formation of the [YCp₂]⁺⁺ fragment with 219.0 *m/z* followed by a subsequent cleavage of an intact Cp unit resulting in the [YCp]⁺⁺ fragment corresponding to 153.9 *m/z* with intensities of 12.5 % and 9.1 % for **1** and **2**, respectively. Another possible fragmentation pathway starting from the molecular ion peak can be proposed through the cleavage of a Cp unit yielding [YCp(R)]⁺⁺ with R = dpamd or dpdmg exhibiting mass to charge ratio values of 295.1 *m/z* and 324.1 *m/z* for **1** and **2**.

Interestingly, these fragments form dimers with intact [M]⁺⁺ species resulting in [(R)CpY-Cp-YCp(R)]⁺⁺. However, the fragments provide either low stability or their formation is unfavorable, which can be seen from the low relative intensities of 0.4 % and 0.3 % for **1** and **2**, respectively. Logically, parallel to the above discussed fragmentation pathways, the subsequently cleaved Cp and amidinate or guanidinate moieties are detected as well exhibiting 65.1 *m/z* for the [Cp]⁺⁺ fragments, 141.1 *m/z* for the [(dpamd)]⁺⁺ and 170.0 *m/z* for the [(dpdmg)]⁺⁺ species.

Hirshfeld Surface Analysis

Hirshfeld surface analysis serves as a valuable tool to study the intermolecular interactions of molecules in crystal structures potentially influencing the physical properties of a compound.^[31]

A Hirshfeld surface visualizes these interactions through the calculation of the ratio between a promolecule (sum of electron densities of spherical atoms forming a molecule) and a procrystal (sum of promolecules) within a crystal cell. In the areas where the ratio exceeds 0.5, the Hirshfeld surface of a molecule can be created as a function of internal (*d_i*), external (*d_e*), or normalized (*d_{norm}*) contact distances using van-der-Waals (vdW)

radii as reference. Due to that, the intermolecular interactions of a molecule within a crystal can be graphically visualized with a 3-dimensional Hirshfeld surface (color scheme represents distances shorter (red) or larger (blue) than vdW radii) as well as a 2-dimensional fingerprint plot (*d_e* vs. *d_i*) highlighting distances of the donor and acceptor atoms with respect to the interactions. It must be considered that this facile analysis tool requires adequately solved crystal structure data with well-solved hydrogen atom positions to yield significant data allowing a statement on the interactions present in the structures.

The calculated 3D Hirshfeld surfaces (*d_{norm}* from -0.1002 to 1.4371) for [YCp₂(dpamd)] **1** and [YCp₂(dpdmg)] **2** as well as the 2D fingerprint maps are depicted in Figure 4. For a comprehensive study of the interactions, the Hirshfeld surfaces and fingerprint maps of the homoleptic counterparts [Y(dpdmg)₃] and [YCp₃] were calculated as well and are presented in the supporting information (Figure S2).

At a first sight, the areas of strong vdW interactions (red spots) shown in the 3D Hirshfeld surfaces are located in similar regions independent of the respective compounds, namely the area of the Cp ligands and the NCN backbone (**1**: CH₃ and **2**: N(CH₃)₂). However, the nature of these interactions differ, focusing on the Cp interactions: For **1**, the acceptor H_{ext}...π(C_{Cp unit}) interaction (2.730 Å) is directed to just one carbon atom within the Cp unit whereas **2** features three distinguishable π interactions of H_{ex} to an interior C_{int}(Cp) with a length of 2.743 Å, 2.745 Å and 2.701 Å, respectively. A similar nature of interaction can be observed at the amine function (N(CH₃)₂) of the backbone of **2** where the H is attracted toward the Cp function of an external molecule, forming either a single or triple interaction from H to the Cp unit. Interestingly, in complex **1** the vdW interactions of an H from the CH₃ backbone moiety to an exterior C of the Cp unit H_{int}...π(C_{ex, Cp unit}) is the analogous donor interaction to the already described acceptor interaction featuring a similar length (2.730 Å). Both complexes **1** and **2** exhibit one additional, pronounced C_{int}...H_{ext} intermolecular interac-

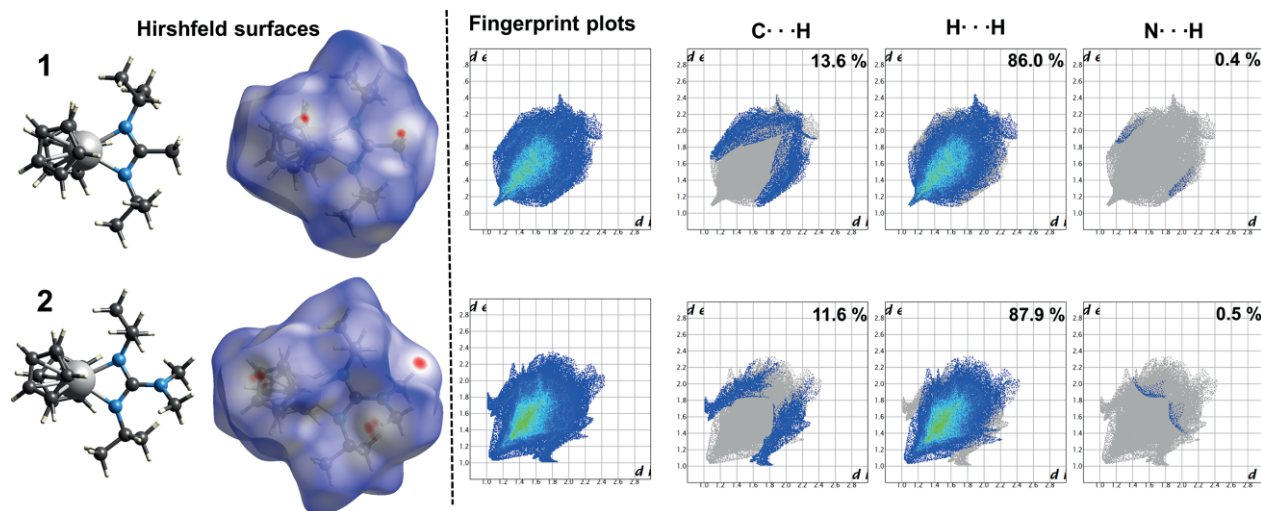


Figure 4. Molecular structures, Hirshfeld surfaces (d_{norm} ranging from -0.1002 \AA red to 1.4371 \AA blue) (left), 2D fingerprint plots (d_i vs. d_e) and decomposed fingerprint plots with relative contributions (right) for compound [YCP₂(dpamd)] **1** and [YCP₂(dpdmg)] **2**.

tion which is located at the second Cp function of the complexes, as visible from the “backside” view of the Hirshfeld surfaces in Figure S4. Surprisingly, it was found out that there is no evidence for strong intermolecular interactions caused by the isopropyl functions. However, the spatial demand of the side chain groups is likely to play a vital role in terms of crystal packing.

The Hirshfeld surfaces of [YCP₃] and [Y(dpdmg)₃] exhibit a completely different situation of intermolecular interactions, with the latter solely featuring two H_{ext}...H_{int} interactions located at either side of the surface. These narrow, 2.025 Å contacts structure the molecules in a “chain-like” orientation within the crystal structure, as visible from Figure S3. Since the [YCP₃] possesses an asymmetric unit cell, the observed vdW interactions for one molecule are rather strong compared to the other compounds. The pronounced, red spot at the Y metal center belongs to the Y_{int}...H_{ext}(Cp) interaction from the closely positioned, second [YCP₃] molecule of the crystal unit cell resulting in the characteristic “zig-zag” structure of the crystal lattice.^[30]

For a quantitative statement, the 2D fingerprint maps and decomposed plots were analyzed for **1** and **2** revealing some notable differences. Generally, the strongest contribution to the intermolecular interactions occur from the H...H contacts with 86.0 % for **1** and 87.9 % for **2** due to the dominant presence of H at the surfaces of the molecules. As seen from the sharp spike at the bottom left of the decomposed H...H fingerprint map of **1**, most short distance H...H contacts feature a similar d_i to d_e value suggesting a similar contribution of the interior and exterior hydrogen atoms to the vdW interactions, whereas for **2** this spike was found to be considerably broader.

Another difference can be seen focusing on the C...H plot of **2** which shows two “wings” located in the acceptor ($d_i + d_e \approx 1.8 \text{ \AA} + 1.0 \text{ \AA}$) and donor region ($d_i + d_e \approx 1.0 \text{ \AA} + 1.8 \text{ \AA}$) of the fingerprint maps referring to the three-fold intermolecular interactions of the respective H... π (C_{Cp unit}) while **1** exhibits more distinct C...H contacts. Interestingly, the overall contribution of C...H interactions was found to be 13.6 % in **1**

but only 11.6 % for **2** which suggests that the amine backbone function lowers the likelihood of intermolecular interactions within the crystal. In addition, both compounds **1** and **2** only exhibit weak N...H interactions (< 1 %) reasoned by the more centered position within the molecule prohibiting a distinct interaction.

In fact, these structural properties for **1** and **2** are in line with the findings of the intermolecular interactions of [Y(dpdmg)₃]. From the fingerprint plots it is shown that solely H...H interactions without the presence of C...H or N...H were calculated, indicating a kind of shielding effect of the guanidinate ligand from the respective hydrogen atoms located at the outer sphere. This is likely to create spatial distance and hinders a strong interaction of C or N with the neighboring H atoms.

From the Hirshfeld surface analysis, the intermolecular interactions of the two different crystal structures of **1** and **2** could be highlighted through the analysis of the interacting molecules within the crystal lattices indicating stronger vdW interactions of **1** because of fewer interactions.

Thermal Properties

Thermogravimetric and differential thermal analysis (TG/DTA) of **1** and **2** were carried out to investigate the thermal properties of the complexes in terms of volatility, thermal stability, and decomposition behavior. Additionally, “stepped” isothermal TG experiments were conducted to estimate the vapor pressures. In order to classify and benchmark the findings for the two heteroleptic compounds, their homoleptic literature known counterparts [YCP₃], [Y(dpamd)₃] and [Y(dpdmg)₃] were measured as well using the same techniques, presented in Figure 5 (TGA), Figure 6 (vapor pressures) and summarized in Table 2, respectively.

As visible from the TG curves, **1** and **2** as well as the homoleptic analogues exhibit a one-step evaporation within the measured temperature range from room temperature to 550 °C.

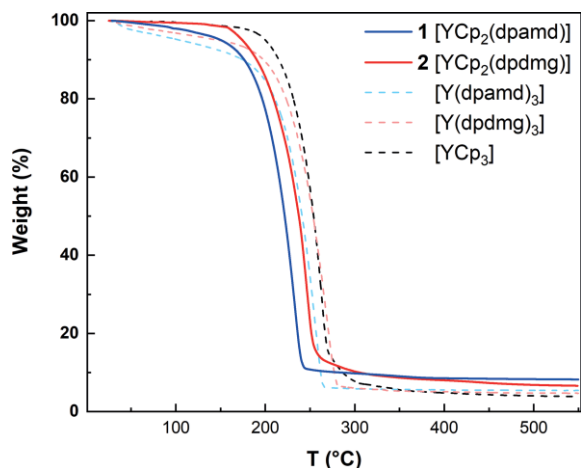


Figure 5. TGA comparison of the heteroleptic $[\text{YCp}_2(\text{dpamd})]$ **1** (blue), $[\text{YCp}_2(\text{dpdmg})]$ **2** (red) with their homoleptic counterparts $[\text{YCp}_3]$ (black), $[\text{Y}(\text{dpamd})_3]$ (light blue) and $[\text{Y}(\text{dpdmg})_3]$ (pink).

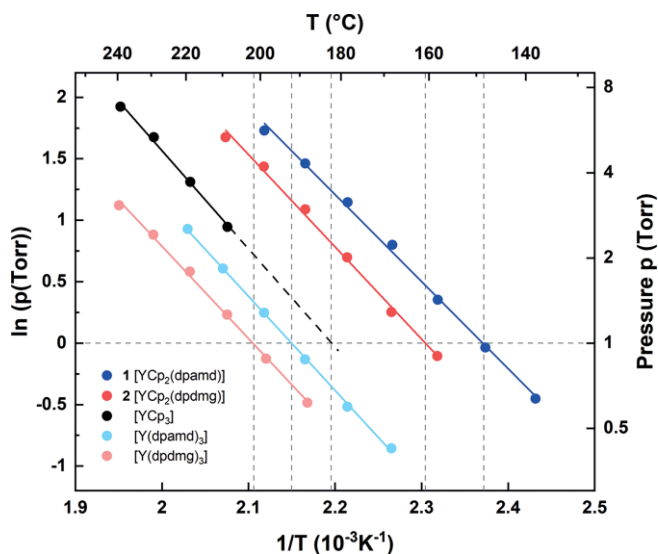


Figure 6. Vapor pressure - temperature functions of the heteroleptic $[\text{YCp}_2(\text{dpamd})]$ **1** (blue), $[\text{YCp}_2(\text{dpdmg})]$ **2** (red), $[\text{Y}(\text{dpamd})_3]$ (light blue), $[\text{Y}(\text{dpdmg})_3]$ (pink) and $[\text{YCp}_3]$ (black). The dashed gray lines are a guidance for the 1 Torr vapor pressure temperatures of the respective compounds.

The onset of volatilization temperature was graphically estimated using the tangential method revealing an apparent trend in the evaporation behavior, rendering $[\text{YCp}_2(\text{dpamd})]$ **1** as the most volatile compound of the series followed by com-

plex $[\text{YCp}_2(\text{dpdmg})]$ **2** whereas all three measured homoleptic complexes require higher temperatures for evaporation.

The rest masses of 8.2 % and 6.6 % for **1** and **2** were found to be slightly higher than the rest masses of the homoleptic analogues which range from 3.9 % – 5.4 %. It must be noted that the presence of rest masses at the end of the TG measurements might be reasoned by the short exposure of the samples to ambient conditions prior to the measurements which could lead to some partial decomposition as the compounds are highly reactive. From the slopes of the TG curves of the compounds it can be assumed that no thermally induced decomposition events occur during the heating process which is confirmed through the absence of exothermic peaks in the DTA curves of **1** and **2** (Figure S5) thus demonstrating the thermal stability of the precursors. For further investigations on the thermal stability, isothermal TG studies of the two heteroleptic precursors **1** and **2** were recorded at 80 °C, 120 °C and 140 °C over a time span of 140 minutes. They can be found in the supporting information (Insets in Figure S5). From these data it is visible that both complexes possess a constant evaporation rate at all measured temperatures without signs of decomposition suggesting a high degree of thermal stability. Furthermore, the evaporation rates of $[\text{YCp}_2(\text{dpamd})]$ **1** were determined to be higher than the rates of $[\text{YCp}_2(\text{dpdmg})]$ **2** at all recorded temperatures following the trend observed in the TG experiments as listed in Table S6.

By analyzing endothermic peaks from the DTA data of all five compounds the respective melting points could be estimated. It was found out that $[\text{YCp}_2(\text{dpdmg})]$ **2** is the complex with the lowest melting point (78.3 °C), followed by $[\text{YCp}_2(\text{dpamd})]$ **1** (97.1 °C). This finding is in line with the observations from Hirshfeld surface analysis showing pronounced vdW interactions for **1** compared to **2** as a consequence of the variation of the NCN backbone function (-CH₃ vs. -N(CH₃)₂) of the N-bonded ligand. $[\text{YCp}_3]$ possesses the highest melting point of all compounds (293.2 °C) reasoned by its strong intermolecular interactions within the asymmetric unit cell such as Y-H and Y- $\pi(\text{C}_{\text{cp}})$ resulting in the characteristic “zig-zag” coordination. However, the comparison of melting points for compounds with different ligand substitution patterns just using the Hirshfeld surface analysis is rather complex which can be seen from the comparison of the melting points of the heteroleptic $[\text{YCp}_2(\text{dpdmg})]$ **2** with the homoleptic analogue $[\text{Y}(\text{dpdmg})_3]$ (117.0 °C). In fact, more structural parameters must be considered to explain the deviation of ca. 20 °C as for instance the higher degree of molecule symmetry.

Table 2. Selected thermal properties of heteroleptic compounds **1**, **2** and the homoleptic analogues $[\text{Y}(\text{dpamd})_3]$, $[\text{Y}(\text{dpdmg})_3]$ and $[\text{YCp}_3]$.

	$[\text{YCp}_2(\text{dpamd})]$ 1	$[\text{YCp}_2(\text{dpdmg})]$ 2	$[\text{Y}(\text{dpamd})_3]$	$[\text{Y}(\text{dpdmg})_3]$	$[\text{YCp}_3]$
Onset of evaporation [°C]	191	203	216	227	224
Residual mass (wt.-%)	8.2	6.6	5.4	4.7	3.9
Melting point [°C]	97.1	78.3	Not detected	117.0	293.2
$T_{\text{vapor pressure}}$ [°C] at $p = 1$ Torr (Standard deviation as error)	148.6 ± 0.6	160.8 ± 0.8	192.0 ± 0.2	201.9 ± 0.4	182.3 ± 1.7
Langmuir equation	$-7082.42 \cdot T^{-1}$	$-7503.41 \cdot T^{-1}$	$-7651.02 \cdot T^{-1}$	$-7507.91 \cdot T^{-1}$	$-8007.18 \cdot T^{-1}$
$\ln(p) = m \cdot T^{-1} + b$	+16.79109	+17.29167	+16.44881	+15.80482	+17.58106
Enthalpy of volatilization ΔH_{V} (kJ mol ⁻¹)	58.89	62.39	63.61	62.42	66.58

The vapor pressure is an important figure of merit to benchmark the thermal properties of metalorganic compounds. In this study, the 1 Torr vapor pressure temperatures of all five presented compounds were estimated from evaporation rates obtained from stepped-isothermal TG data which were correlated with the Langmuir equation. This technique was described by Kunte et al.^[32] and is described in more detail in Scheme S1 of the supporting information.

As illustrated in the vapor pressure graphs it can be seen that precursors **1** and **2** feature the lowest 1 Torr vapor pressure temperatures among all evaluated precursors in this study exhibiting values of (148.6 ± 0.6) °C and (160.8 ± 0.8) °C whereas the homoleptic counterparts $[Y(dpamd)_3]$ (192.0 ± 0.2) °C, $[Y(dpdmg)_3]$ (201.9 ± 0.4) °C and $[Y(Cp)_3]$ (182.3 ± 1.7) °C require higher temperatures for evaporation. In addition, all amidinate substituted complexes possess lower vapor pressures, than their guanidinate substituted counterparts which is valid for both, the heteroleptic and homoleptic complexes. This trend is in line with the other investigated thermal properties such as the onset of volatilization temperatures as well as the melting points demonstrating the potential influence of the structure on the thermal characteristics. With the help of the Clausius-Clapeyron equation, the enthalpy of volatilization ΔH_V was calculated using the correlation of the slope of the vapor pressure curve which equals $(1000 \cdot \Delta H_V / R)$ with R being the gas constant. The obtained values are in a similar range between 58.89 kJ/mol for $[Y(Cp)_2(dpamd)]$ **1** to 63.61 kJ/mol for the homoleptic $[Y(dpamd)_3]$ whereas ΔH_V of $[Y(Cp)_3]$ was found to be slightly increased (66.58 kJ/mol) possibly reasoned by the intermolecular interactions of the Cp rings.

With the structural information obtained from analysis techniques such as single-crystal X-ray diffraction and Hirshfeld surface analysis, we were able to highlight similarities and differences between two heteroleptic precursors $[Y(Cp)_2(dpamd)]$ and $[Y(Cp)_2(dpdmg)]$ impacting the physicochemical properties of the compounds which are important factors for their potential to serve as ALD precursors. The thorough thermal evaluation of the respective compounds and their homoleptic, ALD-proven counterparts $[Y(dpamd)_3]$, $[Y(dpdmg)_3]$ and $[Y(Cp)_3]$ provided insights on the influence of ligand choice and substitution on thermal properties of the resulting precursors. Adopting such an approach to analyze the influence of structure on physicochemical attributes and comparing similar precursor substitutions with each other is expected to open up new strategies for improved precursor development.

Conclusion

Two closely related heteroleptic Y complexes bearing two Cp ligands together with the chelating amidinate $[Y(Cp)_2(dpamd)]$ **1** and guanidinate moieties $[Y(Cp)_2(dpdmg)]$ **2** were successfully synthesized and characterized with the goal of expanding the library of suitable yttrium precursors for ALD. Both complexes exist as monomers in the solid state and in solution, featuring a similar structural situation, which was found to be mostly influenced by the differing NCN backbone functions affecting the bond angles in the bent sandwich like complexes. Mass spec-

trometry confirmed the structure of the compounds which were found to be stable under harsh ionization conditions. Using Hirshfeld surface analysis, the specific interactions of the compounds was evaluated showing stronger pronounced $H \cdots \pi(C_{Cp \text{ unit}})$ interactions for **1** compared to **2**.

From the detailed thermal analysis, suitable volatility and thermal stability could be inferred. A comparative study was performed with the established homoleptic counterparts $[Y(dpamd)_3]$, $[Y(dpdmg)_3]$ and $[Y(Cp)_3]$, revealing $[Y(Cp)_2(dpamd)]$ **1** as the precursor with the most promising thermal properties providing a low 1 Torr vapor pressure temperature (154.2 °C \pm 0.5 °C), which can partially be explained by the effect and influence of intermolecular interactions. Thus, the advantage of heteroleptic complex design was studied highlighting the synergetic effect of thermally stable Cp combined with the volatility of the amidinate and guanidinate ligands. The promising physicochemical properties of this class of precursors indicate their potential and suitability for ALD of Y_2O_3 which is the focus of our ongoing study. Furthermore, we will investigate the effect of homoleptic and heteroleptic precursor substitutions on the ALD film growth characteristics to unravel the chemistry behind ALD precursors.

Experimental Section

General Considerations: Compounds **1** and **2** were synthesized using the following starting materials: Na (Acros), dicyclopentadiene (Sigma Aldrich), YCl_3 (abcr), *N,N'*-diisopropylcarbodiimide (Acros), $LiNMe_2$ (Sigma Aldrich) and methyllithium (Sigma Aldrich). All synthesis procedures were performed using standard Schlenk techniques. NaCp was synthesized following the improved synthesis route of Panda et al.^[33] The lithiated amidinate and guanidinate ligands $[Li(dpamd)]$ and $[Li(dpdmg)]$ were prepared according to established routes.^[34] The synthesis of the target compound **1** was performed following a procedure reported in a patent.^[27]

2.64 g (30 mmol) NaCp was solved in THF and added to a slurry of 2.93 g (15 mmol) YCl_3 in THF and stirred for 4 h followed by the addition of the respective lithiated amidinate $[Li(dpamd)]$ or lithiated guanidinate $[Li(dpdmg)]$ ligand (15 mmol) to the formed $[Y(Cp)_2Cl]_2$ intermediate. The resulting mixture was stirred overnight before all solvents were removed in vacuo. The crude product was extracted and recrystallized from *n*-hexane yielding colorless crystals of **1** and **2**, respectively. For further purification, the products were sublimed at 120 °C under vacuum.

Compound 1 $[Y(Cp)_2(dpamd)]$: Yield: 2.43 g (45 % based on YCl_3), Elemental analysis: $YC_{18}H_{27}N_2$; Calculated: N: 7.77 %, C: 59.99 %, H: 7.55 %, Found: N: 7.74 %, C: 57.90 %, H: 6.57 %, 1H -NMR (300 MHz, C_6D_6): δ [ppm] = 6.20 (s, 9 H, $\{Y(C_5H_5)_2\}$), 3.25 (dsept, $J = 6.3$ Hz, 2.0 Hz, $\{NCH(CH_3)_2\}$), 1.44 (s, 3 H, $\{NC(CH_3)N\}$), 0.93 (d, 12 H, $J = 6.3$ Hz, $\{NCH(CH_3)_2\}$), EI-MS (70 eV): m/z (rel. int. %) [fragment]: 655.3 (0.4 %) $[Y_2(Cp)_3(dpamd)_2]^{++}$, 512.4 (1.4 %) $[Y_2(Cp)_3(dpamd - CH_3)]^{++}$, 469.3 (2.4 %) $[Y_2(Cp)_3(dpamd - CH_3 - iPr)]^{++}$, 360.2 (52.3 %) $[Y(Cp)_2(dpamd)]^{++}$, 345.2 (100.0 %) $[Y(Cp)_2(dpamd - CH_3)]^{++}$, 295.1 (71.4 %) $[Y(Cp)(dpamd)]^{++}$, 279.1 (19.1 %) $[Y(Cp)(dpamd - CH_3)]^{++}$, 219.0 (42.5 %) $[Y(Cp)_2]^{++}$, 210.0 (12.5 %) $[Y(Cp)(dpamd - 2 iPr)]^{++}$, 169.0 (27.3 %) $[Y(Cp)(N)]^{++}$, 154.0 (9.5 %) $[Y(Cp)]^{++}$, 65.1 (1.5 %) $[Cp]^{++}$, 42.0 (12.8 %) $[iPr]^{++}$.

Compound 2 [Y(Cp)₂(dpdmg)]: Yield: 3.04 g (52 % based on YCl₃), Elemental analysis: YC₁₉H₃₀N₃: Calculated: N: 10.79 %, C: 58.61 %, H: 7.77 %, Found: N: 10.71 %, C: 56.81 %, H: 7.10 %, ¹H-NMR (300 MHz, C₆D₆): δ [ppm] = 6.24 (s, 8 H, {Y(C₅H₅)₂}), 3.39 (dsept, *J* = 6.3 Hz, 2.1 Hz, 2 H, {NCH(CH₃)₂}), 2.35 (s, 6 H, {N(CH₃)₂}), 0.95 (d, *J* = 6.3 Hz, 12 H, {NCH(CH₃)₂}), EI-MS (70 eV): *m/z* (rel. int. %) [fragment]: 713.4 (0.3 %) [Y₂(Cp)₃(dpdmg)₂]⁺, 515.1 (1.4 %) [Y₂(Cp)₃(dpdmg - *iPr*)]⁺, 389.2 (59.6 %) [Y(Cp)₂(dpdmg)]⁺, 374.2 (79.6 %) [Y(Cp)₂(dpdmg - CH₃)]⁺, 346.1 (46.0 %) [Y(Cp)₂(dpdmg - *iPr*)]⁺, 324.1 (20.6 %) [Y(Cp)(dpdmg)]⁺, 281.1 (91.4 %) [Y(Cp)(dpdmg - *iPr*)]⁺, 219.0 (100 %) [Y(Cp)₂]⁺, 169.0 (25.3 %) [dpdmg]⁺, 154.0 (9.1 %) [Y(Cp)]⁺, 71.1 (16.7 %) [dpdmg - N - 2 *iPr*]⁺.

Precursor Characterization: X-ray diffraction intensities for **1** were collected on an Agilent Technologies SuperNova diffractometer with an Atlas CCD, using Cu K_α radiation (λ = 1.54184 Å). Single-crystals of complex **2** were measured on an Oxford X-calibur 2 diffractometer using a Mo K_α radiation (λ = 0.71073 Å). For both compounds, the crystals were coated with perfluoropolyether and mounted in a cooled N₂ stream of the diffractometer on a looping system. Diffraction data was calculated with CrysAlisPro.^[35] Molecular structures were solved and refined with the program package SHELXL^[36] using the programs SHELXS-97^[37] and SHELXL-2014.^[38] Crystallographic details are listed in the Supporting Information. ¹H-NMR spectra were measured on a Bruker AVIII 300 instrument. 3D Hirshfeld surfaces and 2D fingerprint plots were generated using the software "CrystalExplorer17"^[39] based on single crystal XRD measurements. The 3D Hirshfeld surface (d_{norm}) illustrates the distance from exterior (d_e) and interior (d_i) atoms to the generated surface with respect to their van der Waals radii. In cases for d_i + d_e being shorter than the sum of vdW radii, the negative value is displayed in red color on the surface whereas blue color indicates a longer range for the sum of d_i and d_e compared to the sum of the vdW radii. The 2D fingerprint plots show d_e as a function of d_i highlighting different types of intermolecular interactions.

Deposition Numbers 1986425 (for **1**) and 1986424 (for **2**) contain the supplementary crystallographic data for this paper. These data are provided free of charge by the joint Cambridge Crystallographic Data Centre and Fachinformationszentrum Karlsruhe Access Structures service www.ccdc.cam.ac.uk/structures.

Electron-impact ionization mass spectra (EI-MS, 70 eV), were recorded operating a VG Instruments Autospec instrument. The output spectra were given as specific mass to charge ratio (*m/z*) based on the abundant isotopes ¹H,¹²C,¹⁴N, and ⁸⁹Y. Elemental analysis was carried out on an Elementar vario MIRCRO-cube instrument from Elementar. Thermogravimetric analyses (TGA) and differential thermogravimetric analysis (DTA) were measured on a Seiko Exstar TG/DTA 6200/SII using 10 mg of sample under a constant N₂ inert gas flow of 300 mL·min⁻¹ and employing a heating rate of 5 °C·min⁻¹. For the estimation of the vapor pressures, "stepped isothermal" TGA were performed with sample masses of approximately 15 mg in a range from 120 °C – 240 °C in 10 °C steps. The steps were held for 10 min at the respective temperatures to allow the evaporation rate to reach an equilibrium.

Acknowledgments

This work was funded by the Federal Ministry of Education and Research, Germany (BMBF, Project 03INT505AB CAP-CPC). The authors thank Dr. Bert Mallick for his support and valuable discussions related to crystal structure determination. Open access funding enabled and organized by Projekt DEAL.

Keywords: Yttrium · Atomic layer deposition · Precursors · Thermal properties · Structure elucidation

- [1] a) Y. Nigara, *Jpn. J. Appl. Phys.* **1968**, *7*, 404–408; b) M. R. Davolos, S. Felicyano, A. M. Pires, R. F. C. Marques, M. Jafelicci, *J. Solid State Chem.* **2003**, *171*, 268–272; c) K. Richardson, M. Akinc, *Ceram. Int.* **1987**, *13*, 253–261.
- [2] a) J. A. Nelson, M. J. Wagner, *Chem. Mater.* **2002**, *14*, 915–917; b) B. Y. Kokuoz, K. Serivalsatit, B. Kokuoz, O. Geiculescu, E. McCormick, J. Ballato, *J. Am. Ceram. Soc.* **2009**, *92*, 2247–2253.
- [3] a) V. H. Mudavakkat, V. V. Atuchin, V. N. Kruchinin, A. Kayani, C. V. Ramana, *Opt. Mater.* **2012**, *34*, 893–900; b) J.-H. Kang, Y. C. Jung, S. Seong, T. Lee, J. Ahn, W. Noh, I.-S. Park, *Mater. Sci. Semicond. Process.* **2017**, *63*, 279–284; c) L. Mai, N. Boysen, E. Subaşı, T. d. I. Arcos, D. Rogalla, G. Grundmeier, C. Bock, H.-L. Lu, A. Devi, *RSC Adv.* **2018**, *8*, 4987–4994; d) A. P. Milanov, K. Xu, S. Cwik, H. Parala, T. de los Arcos, H.-W. Becker, D. Rogalla, R. Cross, S. Paul, A. Devi, *Dalton Trans.* **2012**, *41*, 13936–13947; e) A. P. Milanov, R. A. Fischer, A. Devi, *Inorg. Chem.* **2008**, *47*, 11405–11416.
- [4] a) M. Ju, Y. Xiao, W. Sun, C. Lu, Y.-y. Yeung, *J. Phys. Chem. C* **2020**, *124*, 2113–2119; b) I. Krutikova, M. Ivanov, A. Murzakaev, K. Nefedova, *Mater. Lett.* **2020**, *265*, 127435.
- [5] a) S. J. Pearce, G. J. Parker, M. D. B. Charlton, J. S. Wilkinson, *J. Vac. Sci. Technol. A* **2010**, *28*, 1388–1392; b) S. Zhang, R. Xiao, *J. Appl. Phys.* **1998**, *83*, 3842–3848.
- [6] a) J. D. Traylor-Kruschwitz, W. T. Pawlewicz, *Appl. Opt.* **1997**, *36*, 2157–2159; b) L. Derbali, M. Dkhili, S. Mezni, S. Zargouni, M. Ouadhour, S. El Whibi, H. Ezzaouia, *J. Mater. Sci. Mater. Electron.* **2019**, *30*, 806–811; c) P. Lei, W. Leroy, B. Dai, J. Zhu, X. Chen, J. Han, D. Depla, *Surf. Coat. Technol.* **2015**, *276*, 39–46.
- [7] a) E. Riemann, L. Young, *Surf. Coat. Technol.* **1973**, *44*, 1044–1049; b) J. Kwo, M. Hong, A. R. Kortan, K. L. Queeney, Y. J. Chabal, R. L. Opila, D. A. Muller, S. N. G. Chu, B. J. Sapjeta, T. S. Lay, J. P. Mannaerts, T. Boone, H. W. Krautter, J. J. Krajewski, A. M. Sergnt, J. M. Rosamilia, *J. Appl. Phys.* **2001**, *89*, 3920–3927.
- [8] a) A. Nandi, S. Ghosh, *JMSRR* **2019**, 1–17, DOI: <https://journaljmsrr.com/index.php/JMSRR/article/view/28843>; b) X. Q. Cao, R. Vassen, D. Stoeber, *J. Eur. Ceram. Soc.* **2004**, *24*, 1–10.
- [9] a) A. Afrasiabi, M. Saremi, A. Kobayashi, *Mater. Sci. Eng. A* **2008**, *478*, 264–269; b) W. Hao, Q. Zhang, C. Xing, F. Guo, M. Yi, X. Zhao, P. Xiao, *J. Eur. Ceram. Soc.* **2019**, *39*, 461–469; c) S. Mahade, D. Zhou, N. Curry, N. Markocsan, P. Nylén, R. Vaßen, *J. Mater. Process. Technol.* **2019**, *264*, 283–294.
- [10] I. K. Igumenov, A. N. Aksenov, *Therm. Eng.* **2017**, *64*, 865–873.
- [11] a) A. K. Singh, T. R. G. Kutty, S. Sinha, *J. Nucl. Mater.* **2012**, *420*, 374–381; b) R. Kawasaki, Y. Umetsu, K. Kurashima, K. Shioda, A. Hirooka, H. Habuka, *Mater. Sci. Semicond. Process.* **2018**, *83*, 211–215.
- [12] a) L. K. Chu, W. C. Lee, M. L. Huang, Y. H. Chang, L. T. Tung, C. C. Chang, Y. J. Lee, J. Kwo, M. Hong, *J. Cryst. Growth* **2009**, *311*, 2195–2198; b) W. H. Chang, P. Chang, W. C. Lee, T. Y. Lai, J. Kwo, C.-H. Hsu, J. M. Hong, M. Hong, *J. Cryst. Growth* **2011**, *323*, 107–110.
- [13] S. Xu, Z. Yao, J. Zhou, M. Du, *Surf. Coat. Technol.* **2018**, *344*, 636–643.
- [14] a) S.-s. Yi, J. S. Bae, B. K. Moon, J. H. Jeong, J.-C. Park, I. W. Kim, *Appl. Phys. Lett.* **2002**, *81*, 3344–3346; b) V. Craciun, J. Howard, E. S. Lambers, R. K. Singh, J. Perriere, *Appl. Phys. A* **1999**, *69*, S535–S538.
- [15] a) C. Durand, C. Dubourdieu, C. Vallée, V. Loup, M. Bonvalot, O. Joubert, H. Roussel, O. Renault, *J. Appl. Phys.* **2004**, *96*, 1719–1729; b) M. V. F. Schlupp, M. Prestat, J. Martynczuk, J. L. M. Rupp, A. Bieberle-Hütter, L. J. Gauckler, *J. Power Sources* **2012**, *202*, 47–55.
- [16] a) C. Zimmermann, O. Bethge, K. Winkler, B. Lutzer, E. Bertagnolli, *Appl. Surf. Sci.* **2016**, *369*, 377–383; b) S. Seppälä, J. Niinistö, M. Mattinen, K. Mizohata, J. Räsänen, W. Noh, M. Ritala, M. Leskelä, *Thin Solid Films* **2018**, *660*, 199–206; c) B. Zhao, F. Mattelaer, G. Rempelberg, J. Dendooven, C. Detavernier, *ACS Appl. Mater. Interfaces* **2020**, *12*, 3179–3187; d) T. Blanquart, M. Kaipio, J. Niinistö, M. Gavagnin, V. Longo, L. Blanquart, C. Lamsalot, W. Noh, H. D. Wanzénböck, M. Ritala, M. Leskelä, *Chem. Vap. Deposits* **2014**, *20*, 217–223; e) J.-S. Lee, W.-H. Kim, I.-K. Oh, M.-K. Kim, G. Lee, C.-W. Lee, J. Park, C. Lamsalot-Matras, W. Noh, H. Kim, *Appl. Surf. Sci.* **2014**, *297*, 16–21; f) I.-S. Park, Y. Chan Jung, S. Seong, J. Ahn, J. Kang, W. Noh,

- C. Lansalot-Matras, *J. Mater. Chem. C* **2014**, *2*, 9240–9247; g) S. Seppälä, J. Niinistö, T. Blanquart, M. Kaipio, K. Mizohata, J. Räisänen, C. Lansalot-Matras, W. Noh, M. Ritala, M. Leskelä, *Chem. Mater.* **2016**, *28*, 5440–5449; h) J. Zhang, R. Cai, L. Weng, X. Zhou, *Organometallics* **2004**, *23*, 3303–3308; i) M. Leskelä, M. Ritala, *J. J. Solid State Chem.* **2003**, *171*, 170–174.
- [17] a) S. M. George, *Chem. Rev.* **2010**, *110*, 111–131; b) R. W. Johnson, A. Hultqvist, S. F. Bent, *Mater. Today* **2014**, *17*, 236–246.
- [18] a) A. Devi, *Coord. Chem. Rev.* **2013**, *257*, 3332–3384; b) M. Leskelä, M. Ritala, *Thin Solid Films* **2002**, *409*, 138–146.
- [19] a) W. J. Evans, *Inorg. Chem.* **2007**, *46*, 3435–3449; b) F. T. Edelmann, *Chem. Soc. Rev.* **2012**, *41*, 7657–7672.
- [20] D. A. Atwood, *The Rare Earth Elements: Fundamentals and Application*; Wiley, Hoboken, NJ, **2012**.
- [21] S. P. Nolan, S. Stern, T. J. Marks, *J. Am. Chem. Soc.* **1989**, *111*, 7844–7853.
- [22] a) M. Håkansson, M. Helin, M. Putkonen, Q. Jiang, M. Kotiranta, J. Suomi, A. J. Niskanen, T. Ala-Kleme, S. Kulmala, *Anal. Chim. Acta* **2005**, *541*, 135–139; b) H. Mösla, L. Niinistö, M. Utriainen, *Adv. Mater. Opt. Electron.* **1994**, *4*, 389–400; c) M. Putkonen, T. Sajavara, L.-S. Johansson, L. Niinistö, *Chem. Vap. Deposition* **2001**, *7*, 44–49.
- [23] a) C. N. Ginestra, R. Sreenivasan, A. Karthikeyan, S. Ramanathan, P. C. McIntyre, *Electrochem. Solid-State Lett.* **2007**, *10*, B161–B165; b) J. Niinistö, M. Putkonen, L. Niinistö, *Chem. Mater.* **2004**, *16*, 2953–2958.
- [24] a) C.-C. Chao, Y. B. Kim, F. B. Prinz, *Nano Lett.* **2009**, *9*, 3626–3628; b) J. H. Shim, C.-C. Chao, H. Huang, F. B. Prinz, *Chem. Mater.* **2007**, *19*, 3850–3854; c) J. H. Shim, J. S. Park, J. An, T. M. Gür, S. Kang, F. B. Prinz, *Chem. Mater.* **2009**, *21*, 3290–3296; d) T. Roessler, J. Gluch, M. Albert, J. W. Bartha, *Thin Solid Films* **2010**, *518*, 4680–4683; e) L. Lecordier, *ECS Trans.* **2015**, *69*, 109–116; f) A. I. Abdulagatov, R. R. Amashaev, K. N. Ashurbekova, S. M. Ramazanov, D. K. Palchaev, A. M. Maksumova, M. K. Rabadanov, I. M. Abdulagatov, *Russ. Microelectron.* **2019**, *48*, 1–12; g) N. A. Stafford, R. Katamreddy, L. Guerin, B. Feist, C. Dussarrat, V. Pallem, C. Weiland, R. Opila in *ECS Transactions*, ECS, **2009**.
- [25] P. de Rouffignac, J.-S. Park, R. G. Gordon, *Chem. Mater.* **2005**, *17*, 4808–4814.
- [26] a) S. Cwik, S. M. J. Beer, S. Hoffmann, M. Krasnopolski, D. Rogalla, H.-W. Becker, D. Peeters, A. Ney, A. Devi, *ACS Appl. Mater. Interfaces* **2017**, *9*, 27036–27044; b) S. Cwik, S. M. J. Beer, M. Schmidt, N. C. Gerhardt, T. de los Arcos, D. Rogalla, J. Weßing, I. Giner, M. Hofmann, G. Grundmeier, A. D. Wieck, A. Devi, *Dalton Trans.* **2019**, *48*, 2926–2938; c) A. P. Milanov, T. Toader, H. Parala, D. Barreca, A. Gasparotto, C. Bock, H.-W. Becker, D. K. Ngwashi, R. Cross, S. Paul, U. Kunze, R. A. Fischer, A. Devi, *Chem. Mater.* **2009**, *21*, 5443–5455.
- [27] V. R. Palem, C. Dussarrat. Preparation of Lanthanide-Containing Precursors and Deposition of Lanthanide-Containing Films(US 8,283,201 B2), Oct. 9.
- [28] G. Wilkinson, J. M. Birmingham, *J. Am. Chem. Soc.* **1956**, *78*, 6210.
- [29] P. Jutzi, T. Redeker, B. Neumann, H.-G. Stammer, *Organometallics* **1996**, *15*, 4153–4161.
- [30] M. Adam, U. Behrens, R. D. Fischer, *Acta Crystallogr., Sect. C* **1991**, *47*, 968–971.
- [31] M. A. Spackman, D. Jayatilaka, *CrystEngComm* **2009**, *11*, 19–32.
- [32] G. V. Kunte, S. A. Shivashankar, A. M. Umarji, *Meas. Sci. Technol.* **2008**, *19*, 25704.
- [33] T. K. Panda, M. T. Gamer, P. W. Roesky, *Organometallics* **2003**, *22*, 877–878.
- [34] a) B. S. Lim, A. Rahtu, J.-S. Park, R. G. Gordon, *Inorg. Chem.* **2003**, *42*, 7951–7958; b) Sarah L. Aeilts, Martyn P. Coles, Dale C. Swenson, and Richard F. Jordan*, and Victor G. Young, Jr.
- [35] *CrysAlisPro Software system*; Agilent Technologies, Oxford, U.K, **2011**.
- [36] C. B. Hübschle, G. M. Sheldrick, B. Dittrich, *J. Appl. Crystallogr.* **2011**, *44*, 1281–1284.
- [37] G. M. Sheldrick, *Acta Crystallogr., Sect. A: Found. Crystallogr.* **2008**, *64*, 112–122.
- [38] G. M. Sheldrick, *Acta Crystallogr., Sect. C: Struct. Chem.* **2015**, *71*, 3–8.
- [39] M. J. Turner, J. J. McKinnon, S. K. Wolff, D. J. Grimwood, P. R. Spackman, Jayatilaka D, M. A. Spackman, *CrystalExplorer17*; University of Western Australia, Crawley, Western Australia (<https://hirshfeldsurface.net>), **2017**.

Received: May 3, 2020